Electronic Supplementary Information

Enhancing Acidic Hydrogen Evolution through Pyrrolic Nitrogen-Doped Reduced Graphene Oxide Triggering Two-Electron Oxygen Reduction

Zhiqiang Hou,[a,‡] Hui Jiang,[a,‡] Yanru Guo,[a] Kejing Huang,[b,*] Fei Zhao,[a] Yongyan Xu,[a] Peng Peng,[a] Shiyu Zou[a,*] Jianjun Yan,[c] Junjun Zhang[d,*]

[a] *School of Chemistry and Chemical Engineering, Zhou Kou Normal University, Henan, 466001, P. R. China.*

[b] *Education Department of Guangxi Zhuang Autonomous Region, Laboratory of Optic-electric Chemo/Biosensing and Molecular Recognition, Guangxi Collaborative Innovation Center for Chemistry and Engineering of Forest Products, Guangxi Key Laboratory of Chemistry and Engineering of Forest Products, Key Laboratory of Chemistry and Engineering of Forest Products, State Ethnic Affairs Commission, School of Chemistry and Chemical Engineering, Guangxi Minzu University, Nanning 530006, China.*

[c] *Journal of Zhou Kou Normal University Editorial Department, Zhou Kou Normal University, Henan, 466001, P. R. China.*

[d] *State Key Laboratory of High-Efficiency Utilization of Coal and Green Chemical Engineering, College of Chemistry & Chemical Engineering, Ningxia University, Yinchuan 750021, Ningxia, P.R. China.*

[*] Corresponding author.

E-mail address: kejinghuang@163.com (K.J. Huang); shiyu_zou@sina.com (S.Y.

Zou); zhangjj089@nxu.edu.cn (J.J. Zhang)

[‡] These authors contributed equally to this work.

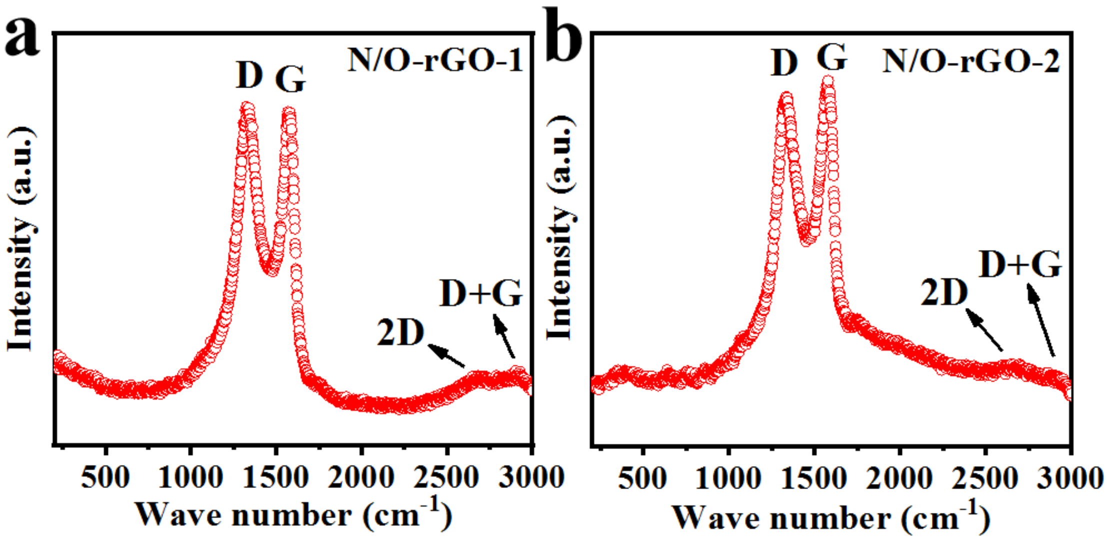

Fig. S1 Roman spectra of (a) N/O-rGO-1 and (b) N/O-rGO-2.

Document: 2024014 (varioELcube) from: –.–.– (modified)

analytic functional testing
vario E Lcube
serial number: 19143037

Text report

No.	Name	N [%]	C [%]	N Area	C Area
64	mo-1 → N/O-rGO-1	0.57	74.36	101	26 230
65	mo-2 → N/O-rGO-2	0.45	73.99	126	35 952

Document: Untitled (VarioMICRO) from: –.--.-- (modified)

LABCAS
test by zhangjun
serial number: 15061010

Text report

	Name	O [%]	O Area	Method
43	MO-2 → N/O-rGO-2	21.144	10 521	Standard
46	MO-1 → N/O-rGO-1	17.959	8 282	Standard

Fig. S2 Elemental analysis tests for N/O-rGO-1 and N/O-rGO-2.

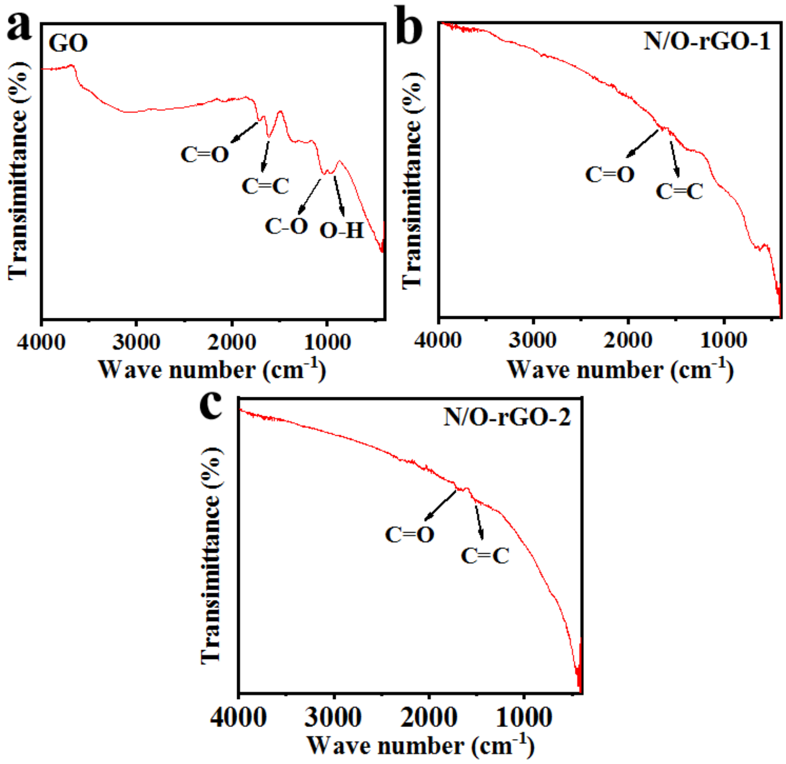

Fig. S3 FTIR spectra of (a) GO, (b) N/O-rGO-1 and (c) N/O-rGO-2.

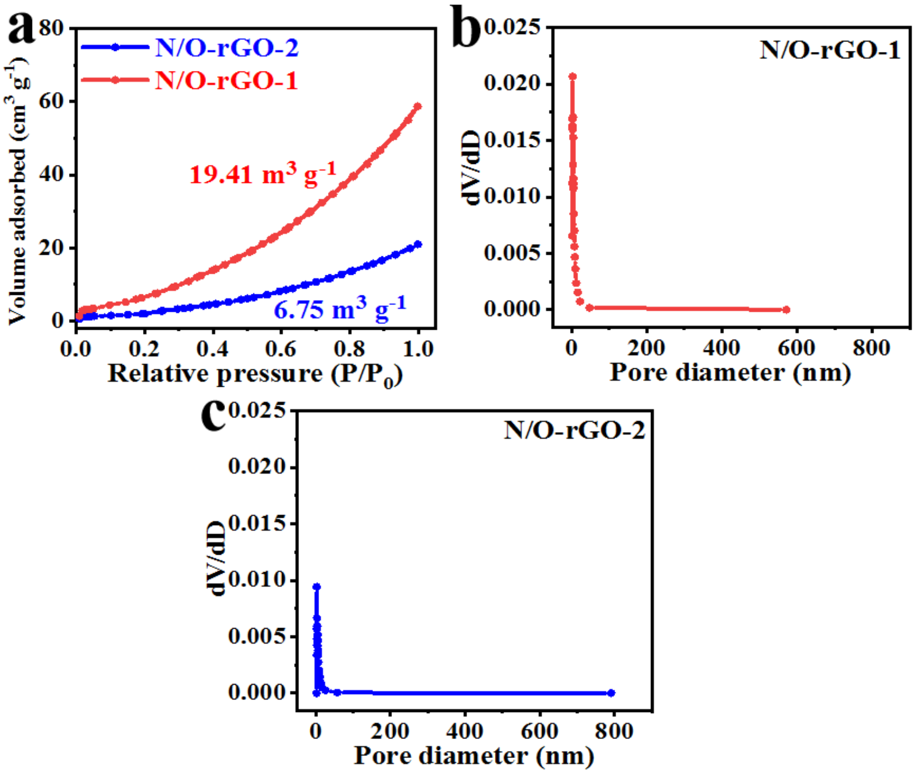

Fig. S4 (a) N_2 adsorption/desorption isotherms and pore size distribution of (b) N/O-rGO-1 and (c) N/O-rGO-2.

The specific surface areas and pore size distribution of N/O-rGO-1 and N/O-rGO-2 were analyzed using a BET analyzer, as depicted in Fig. S4. The N_2 adsorption and desorption curves of N/O-rGO-1 and N/O-rGO-2 exhibit type III isotherms (Fig. S4a). The analysis results suggest that N/O-rGO-1 has a higher BET specific surface area (19.41 m^3 g^{-1}) than N/O-rGO-2, providing rich reactive active sites. Furthermore, N/O-rGO-1 also shows a much more micropore and mesopore structure compared to N/O-rGO-2 (Fig. S4b and S4c), which is beneficial for improving electrochemical performance [S1].

[S1] Y. F. Wang, S. J. Zou, W. P. Hu, F. F. Wu, J. X. Yang, Y. Y. Cen, D. X. Yang, Z. Q. Hou, K. J. Huang, Biomass-derived graphene-like carbon nanoflakes for advanced supercapacitor and hydrogen evolution reaction, *J. Alloy. Compd.*, 2022, **928**, 167176.

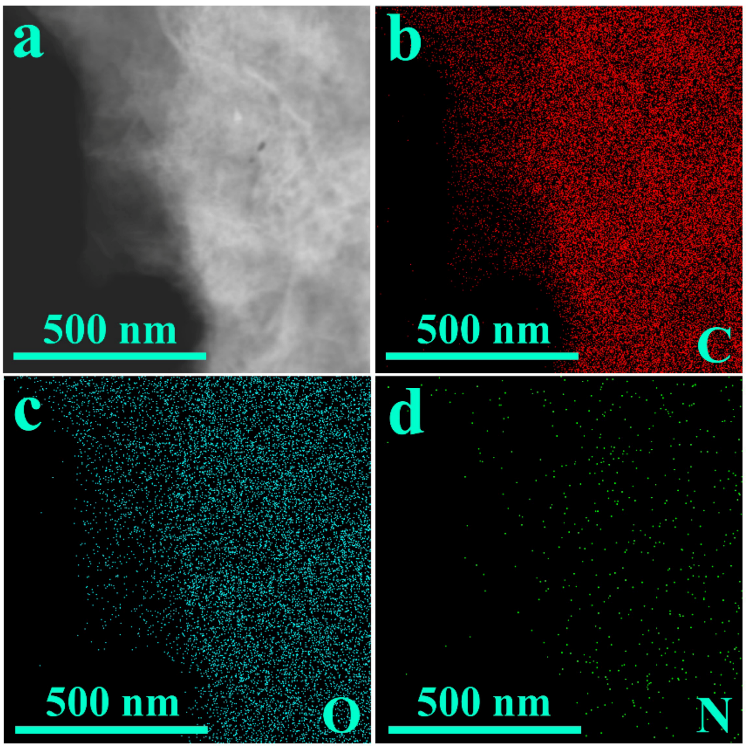

Fig. S5 EDS mapping test for N/O-rGO-1.

Fig. S6 An electrolytic cell with close electrode spacing.

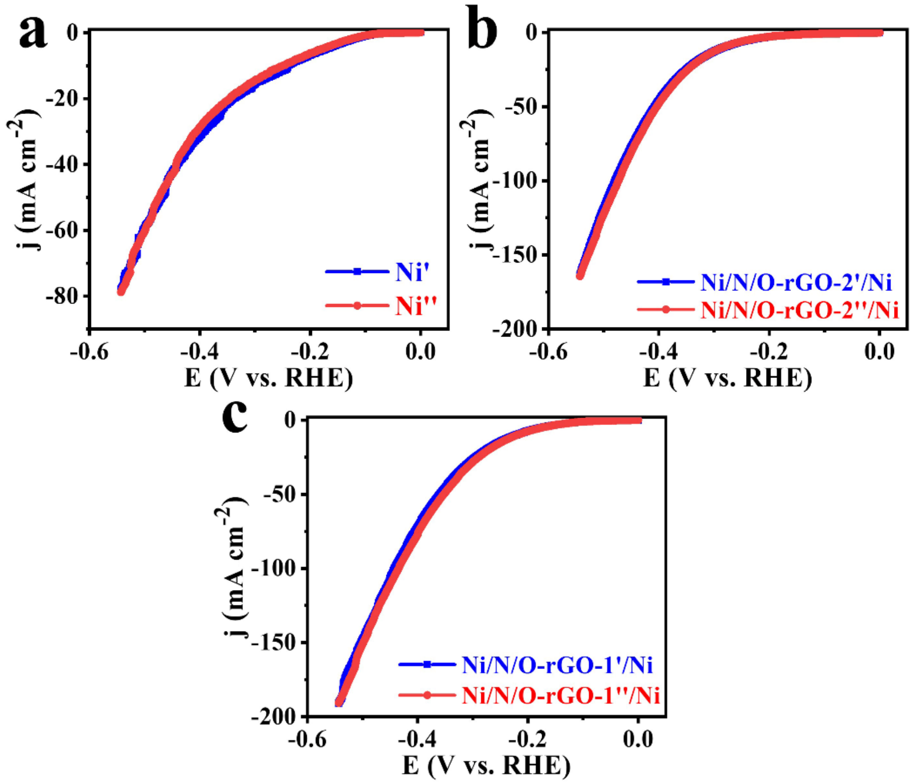

Fig. S7 The duplicate LSV tests for (a) Ni, (b) Ni/N/O-rGO-2/Ni, and (c) Ni/N/O-rGO-1/Ni.

Table S1 Comparison of Ni/N/O-rGO/Ni with previous related research of precursor, method to synthesis, crystalline phase, and catalyst efficiency.

Catalyst	Precursor	Synthetic method	η_{10} (mV)	Ref.
$NiFe_2O_4$@N-rGO-CC	$NiCl_2·6H_2O$, $FeCl_3·6H_2O$, GO solution, et al	Hydrothermal and thermal treatment	188	[S2]
Mo_2C/MoN/NG	Dicyandiamide and $(NH_4)_6Mo_7O_{24}$	Thermal treatment	78.82	[S3]
$Fe_1Co_2Ni_1P$/VrGO	$FeSO_4·7H_2O$, $Ni(NO_3)_2·6H_2O$, et al	Electroless plating	139	[S4]
IrO_2-RuO_2/C	$RuCl_3·xH_2O$, $H_2IrCl_6·6H_2O$, N-doped carbon, et al	Microwave treatment, thermal treatment, et al	82	[S5]
A-NGO-Pt	GO solution, H_2PtCl_6, et al	Hydrothermal and thermal treatment	59	[S6]
Ni/N/O-rGO-1/Ni	GO solution	Hydrothermal and thermal treatment	229	This work

[S2] K. Zhang, P. Jiang, Q. Gu, Y. Leng and P. Zhang, Design of a high-efficiency bifunctional electrocatalyst: Rich-nitrogen-doped reduced graphene oxide-modified carbon cloth-growing nickel-iron complex oxides for overall water splitting. *Energy Fuel*, 2022, **36**, 4911-4923.

[S3] J. Wang, W. Chen, T. Wang, N. Bate, C. Wang and E. Wang, A strategy for highly dispersed Mo_2C/MoN hybrid nitrogen-doped graphene via ion-exchange resin synthesis for efficient electrocatalytic hydrogen reduction. *Nano Res*., 2018, **11**, 4535-4548.

[S4] K. Guo, F. Shaik, J. Yang and B. Jing, Tuning the cationic ratio of $Fe_1Co_xNi_yP$

integrated on vertically aligned reduced graphene oxide array via electroless plating as efficient self-supported bifunctional electrocatalyst for water splitting. *J. Electrochem. En. Conv. Stor.*, 2022, **19**, 021010(1-13).

[S5] R. Samanta, P. Panda, R. Mishra and S. Barman, IrO_2-modified RuO_2 nanowires/nitrogen-doped carbon composite for effective overall water splitting in all pH. *Energy Fuel*, 2022, **36**, 1015−1026.

[S6] M. Saquib, A. Bharadwaj, H. S. Kushwaha and A. Halder, Chloride corrosion resistant nitrogen doped reduced graphene oxide/platinum electrocatalyst for hydrogen evolution reaction in an acidic medium. *ChemistrySelect*, 2020, **5**, 1739-1750.

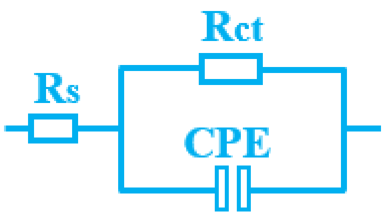

Fig. S8 The fitted equivalent circuits of the Nyquist plots for Ni plate.

Table S2 The parameter of Rs, Rct, CPE, and W for the Ni/N/O-rGO-1/Ni, Ni/N/O-rGO-2/Ni, and Ni plate electrode.

Electrode	Rs (Ω)	Rct	CPE	W
Ni/N/O-rGO-1/Ni	0.759	1.845	0.00129	0.1804
Ni/N/O-rGO-2/Ni	0.760	2.498	0.00152	0.120
Ni	1.291	20.55	0.0005	------

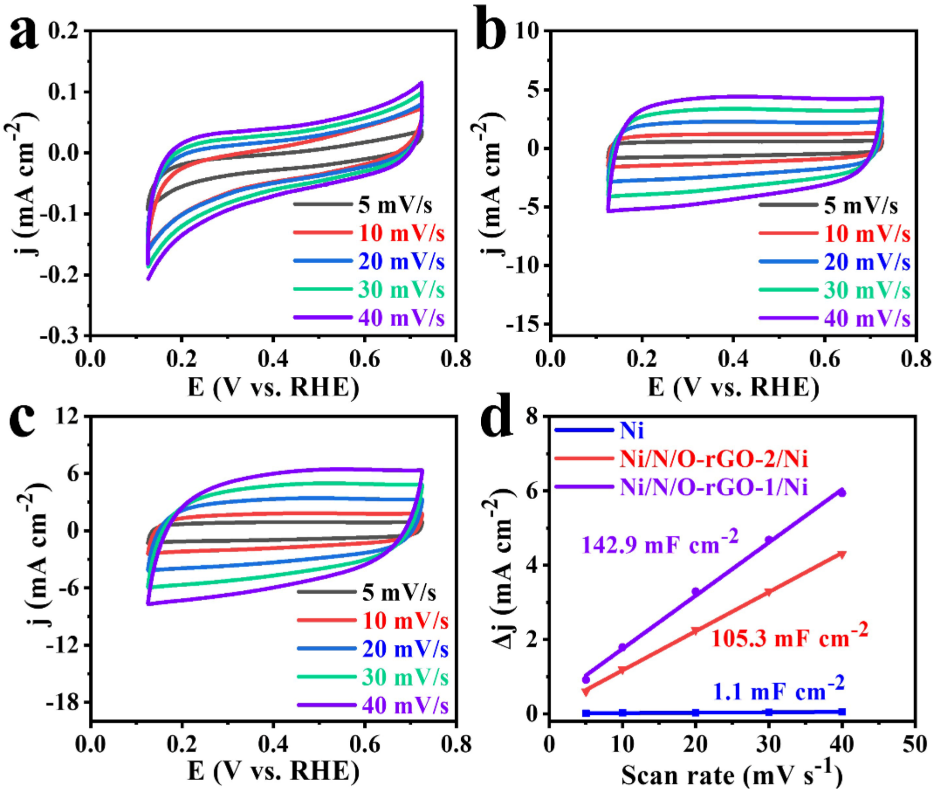

Fig. S9 CV curves of (a) Ni, (b) Ni/N/O-rGO-2/Ni, and (c) Ni/N/O-rGO-1/Ni. (d) Plots of capacitive currents as a function of scan rate for Ni, Ni/N/O-rGO-2/Ni, and Ni/N/O-rGO-1/Ni.

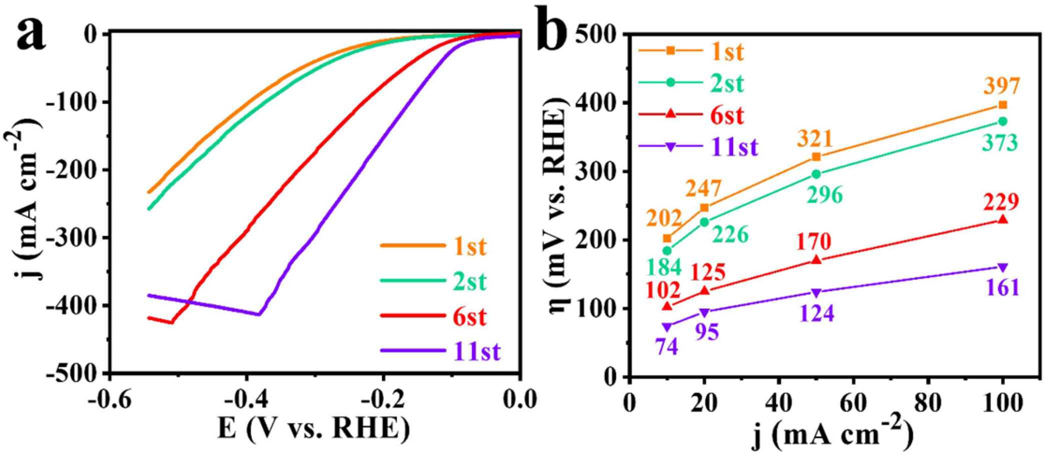

Fig. S10 LCV curves of Ni/N/O-rGO-1/Ni after the 1st, 2nd, 6th, and 11th chronopotentiometry tests in a 275-hour electrocatalytic life.

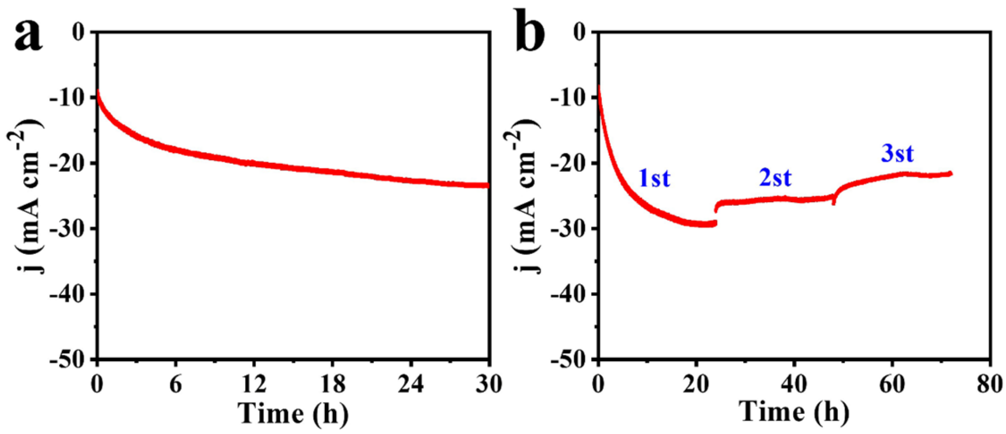

Fig. S11 Chronopotentiometry of Ni/N/O-rGO-2/Ni and Ni.

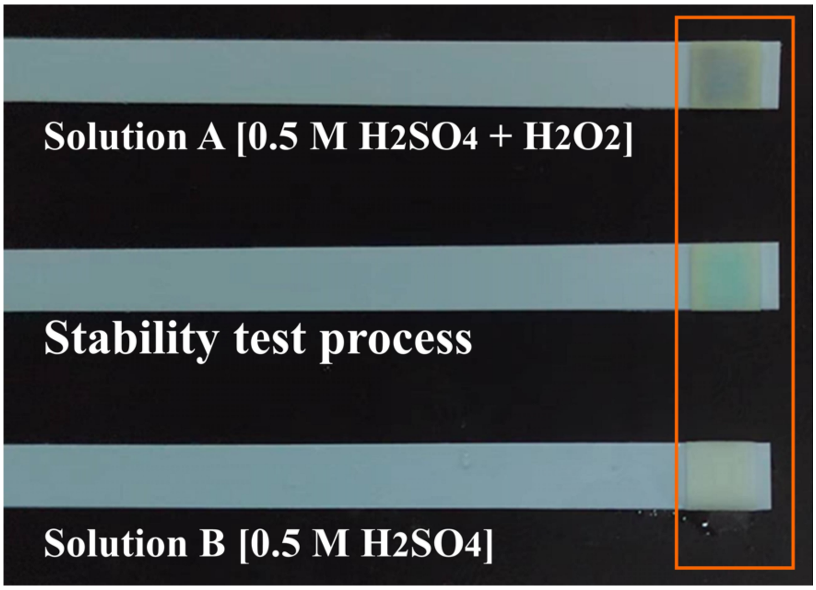

Fig. S12 Verify the presence of H_2O_2 species using the H_2O_2 detection test paper.

We employed H_2O_2 detection test papers (Zhejiang Lohand Environment Technology Co. Ltd, 1-100 mg/L) to determine the presence of H_2O_2 species in the electrocatalysis durability assessment. Fig. S12 demonstrates that the colorimetric response of the test paper indicates the presence of H_2O_2 throughout the stability assessment. In comparison, the detection test paper exhibits a darker hue compared to its appearance during the stability assessment, attributed to Solution A's higher H_2O_2 concentration. Furthermore, the lack of color change in the detection test paper for

Solution B (0.5 M H_2SO_4) confirms H_2O_2's absence.

Fig. S13 An H-type electrolytic cell with a longer electrode spacing.

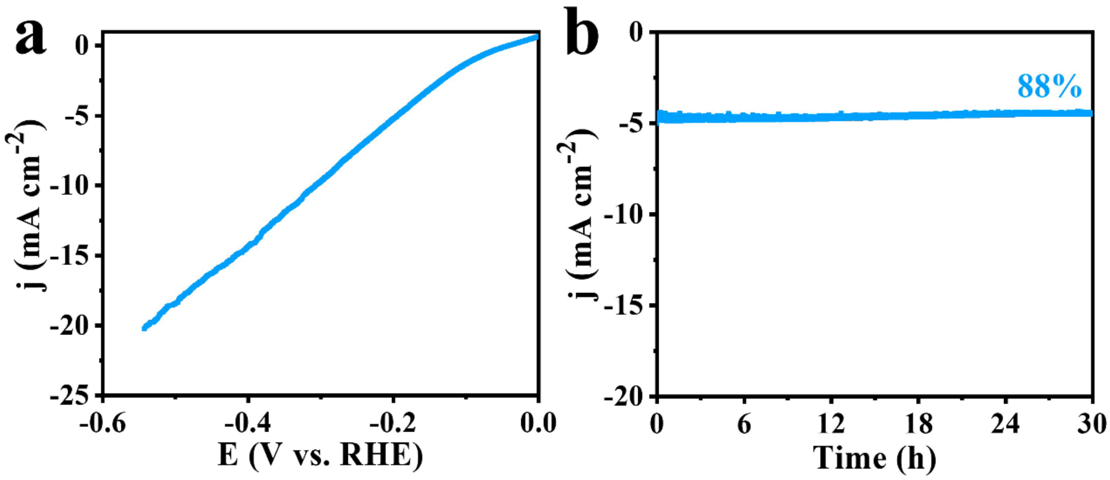

Fig. S14 LSV curves and chronopotentiometry of Ni/N/O-rGO-1/Ni using an H-type electrolytic cell.

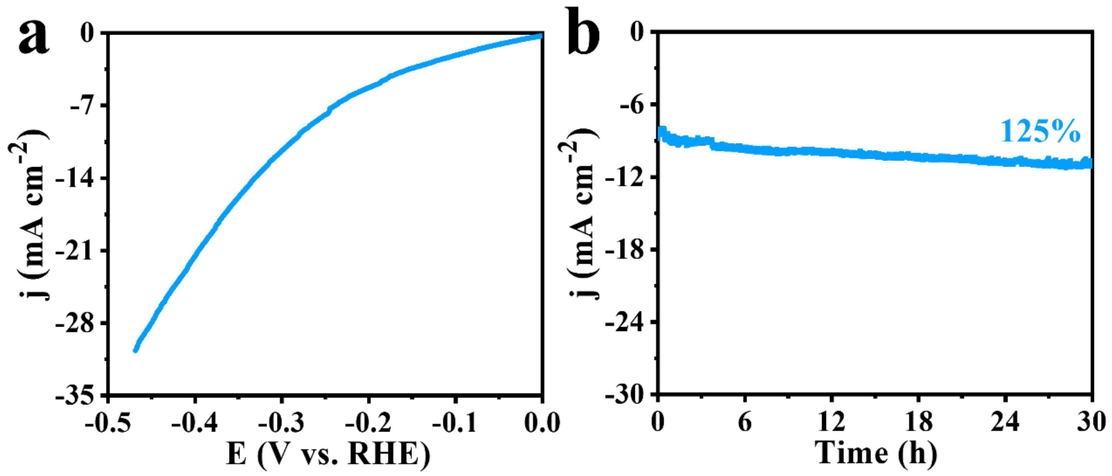

Fig. S15 LSV curves and chronopotentiometry of Ni/N/O-rGO-1/Ni in 0.4 M H_3PO_4 solution.

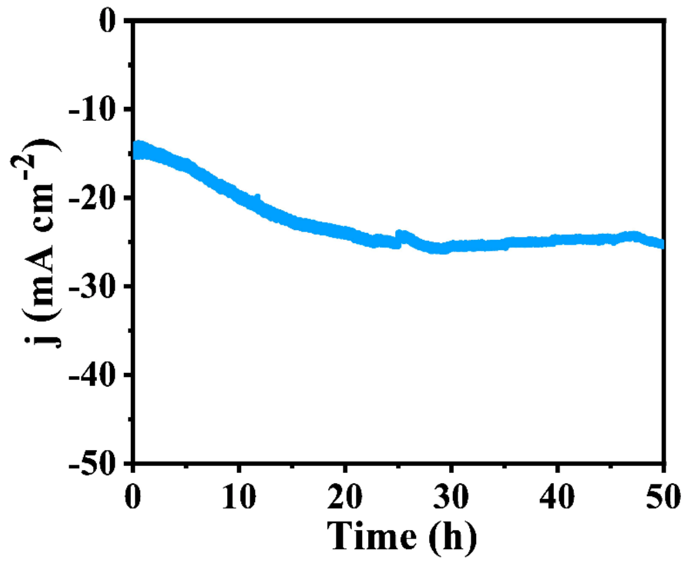

Fig. S16 Chronopotentiometry of Ni/N/O-rGO-1/Ni in 0.5 M H_2SO_4 solution at 20 °C.